Crystal structure of the Borna disease virus matrix protein (BDV-M) reveals ssRNA binding properties

Piotr Neumann[a,1], Diana Lieber[a,2], Sylke Meyer[a], Philipp Dautel[a], Andreas Kerth[b], Ina Kraus[c,3], Wolfgang Garten[c], and Milton T. Stubbs[a,d,4]

[a]Institut für Biochemie und Biotechnologie and [d]Mitteldeutsches Zentrum für Struktur und Dynamik der Proteine, Martin-Luther-Universität Halle-Wittenberg, Kurt-Mothes-Straße 3, D-06120 Halle (Saale), Germany; [b]Institut für Chemie, Martin-Luther-Universität Halle-Wittenberg, Mühlpforte 1, D-06108 Halle (Saale), Germany; and [c]Institut für Virologie, Philipps-Universität Marburg, Hans-Meerwein-Straße 2, D-35047 Marburg, Germany

Edited by Peter Palese, Mount Sinai School of Medicine, New York, NY, and approved January 23, 2009 (received for review September 8, 2008)

Borna disease virus (BDV) is a neurotropic enveloped RNA virus that causes a noncytolytic, persistent infection of the central nervous system in mammals. BDV belongs to the order *Mononegavirales*, which also includes the negative-strand RNA viruses (NSVs) Ebola, Marburg, vesicular stomatitis, rabies, mumps, and measles. BDV-M, the matrix protein (M-protein) of BDV, is the smallest M-protein (16.2 kDa) among the NSVs. M-proteins play a critical role in virus assembly and budding, mediating the interaction between the viral capsid, envelope, and glycoprotein spikes, and are as such responsible for the structural stability and individual form of virus particles. Here, we report the 3D structure of BDV-M, a full-length M-protein structure from a nonsegmented RNA NSV. The BDV-M monomer exhibits structural similarity to the N-terminal domain of the Ebola M-protein (VP40), while the surface charge of the tetramer provides clues to the membrane association of BDV-M. Additional electron density in the crystal reveals the presence of bound nucleic acid, interpreted as cytidine-5′-monophosphate. The heterologously expressed BDV-M copurifies with and protects ssRNA oligonucleotides of a median length of 16 nt taken up from the expression host. The results presented here show that BDV-M would be able to bind RNA and lipid membranes simultaneously, expanding the repertoire of M-protein functionalities.

membrane binding | peripheral membrane protein

Pathological infection with Borna disease virus (BDV) reveals itself in behavioral abnormalities followed by neurological signs of motor system dysfunction, including paralysis (1–3). The disease (named after the village of Borna near Leipzig in Germany, where the first epidemic was described in the Saxon cavalry in the 19th century) affects mainly horses and sheep, but has also been reported in farm animals such as other *Equidae*, cattle, goats, and rabbits or in companion animals, e.g., dogs, cats, or zoo animals (2). Wild rodents such as shrews have been suggested to act as a potential reservoir species responsible for accidental infections of other species (4). Although it has also been suggested that BDV may infect humans and might be associated with certain neuropsychiatric disorders (2), this idea is highly controversial (5). Nonetheless, experimental infection with BDV serves as an important model system for the investigation of viral persistence in the central nervous system and its associated disorders (1, 2, 6).

BDV is an enveloped virus with a nonsegmented, negative-strand RNA genome (7). Six partially overlapping ORFs encode proteins that form a virus particle of spherical morphology and a diameter ranging from 70 to 130 nm. BDV belongs to the order *Mononegavirales*, which also includes the *Filoviridae* (classified into 2 species, Ebola and Marburg viruses), the *Rhabdoviridae* [with prominent members vesicular stomatitis virus (VSV) and rabies virus] and *Paramyxoviridae* (including mumps and measles viruses). The unique biological features of BDV of nuclear replication and transcription, usage of the RNA-splicing machinery of the host cell and the 8.9-kb genome, which is the smallest and most compact of all viruses in this order, warrant the separate taxonomic family *Bornaviridae* (7).

Viral matrix proteins (M-proteins) play a critical role during the process of assembly and budding, because they interact with the cytoplasmic part of the glycoprotein in the cellular membrane (8). M-proteins of several negative-strand RNA viruses (NSVs) are also involved in the regulation of virus replication and transcription and in the transport of ribonucleoprotein (RNP) complexes (9–13). BDV-M, the M-protein of BDV, is the smallest M-protein (16.2 kDa) among all NSVs. It is located beneath the viral envelope and associates with the inner layer of the viral membrane and as such is responsible for the structural integrity and individual form of virus particles by bridging the nucleocapsid and the envelope (14). BDV-M forms oligomers both in vivo and in vitro, with tetramers as the most stable structural unit (15, 16). The tetramers are noncovalently associated and can form 2D lattice-like structures (16); analytical ultracentrifugation and electron microscopic analysis also indicate higher-order association states of the tetrameric BDV-M.

Structures of protease-resistant M-protein fragments from 3 NSVs have been reported to date: VP40 from Ebola virus (17, 18), M from VSV (19), and M1 from influenza virus (20, 21). These M-proteins exhibit neither sequence nor structural homology to one other (10). Here, we report the 3D structure of BDV-M, a full-length M-protein structure of a nonsegmented NSV, and show that the peripheral membrane protein binds ssRNA oligonucleotides.

Results

Structure of the BDV-M Monomer. The BDV-M monomer (Fig. 1), with dimensions 44 × 40 × 40 Å, folds into an L-shaped β-sandwich consisting of 6 antiparallel strands arranged in 2 β-sheets of 3 strands in each (β-sheet I consisting of strands β1, β2, and β6, and β-sheet II composed of strands β3, β4, and β5). The β-strands are slightly bent and concavely twisted (Fig. 1*A*).

Author contributions: W.G. and M.T.S. designed research; P.N., D.L., S.M., P.D., A.K., I.K., and M.T.S. performed research; S.M., A.K., and I.K. contributed new reagents/analytic tools; P.N., A.K., W.G., and M.T.S. analyzed data; and P.N., D.L., W.G., and M.T.S. wrote the paper.

The authors declare no conflict of interest.

This article is a PNAS Direct Submission.

Data deposition: The atomic coordinates have been deposited in the Protein Data Bank, www.pdb.org (PDB ID code 3F1J).

[1]On leave from: Wydział Chemii, Uniwersytet Mikołaja Kopernika, Gagarina 7, 87-100 Torun, Poland.

[2]Present address: Laboratoire de Biologie Chimique, Institut de Science et d'Ingénierie Supramoléculaires, 8, Allée Gaspard Monge, BP 70028, F-67083 Strasbourg Cedex, Strasbourg, France.

[3]Present address: Bundesforschungsanstalt für Ernährung und Lebensmittel, Institut für Biochemie und Physiologie der Ernährung, Hermann-Weigmann-Strasse 1, D-24103 Kiel, Germany.

[4]To whom correspondence should be addressed. E-mail: stubbs@biochemtech.uni-halle.de.

This article contains supporting information online at www.pnas.org/cgi/content/full/0808101106/DCSupplemental.

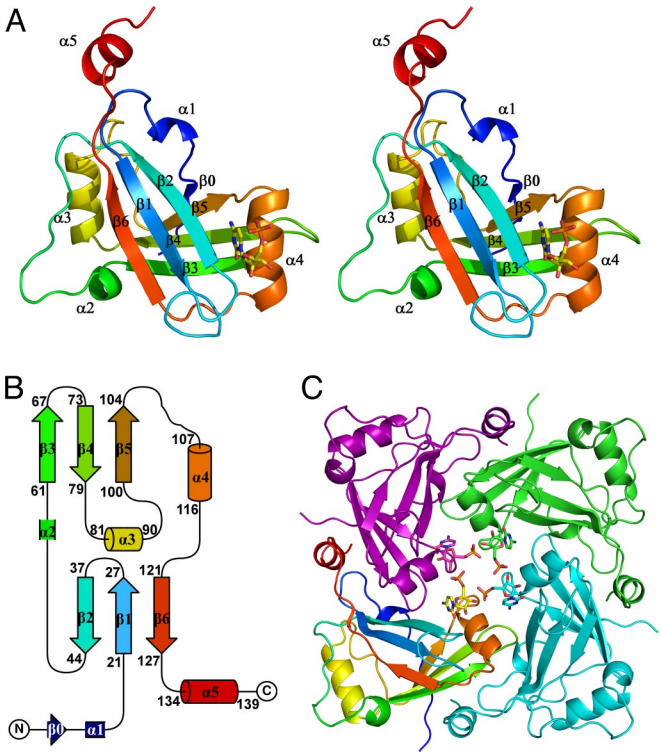

Fig. 1. Overall structure of BDV-M. (*A*) The BDV-M monomer, rainbow-colored from the N to the C terminus. The position of the bound ribonucleotide (cytidine–5′-monophosphate) is indicated in stick representation. (*B*) Topology of the BDV-M monomer with residue numbers of secondary structure elements (β-strands as arrows, α-helices as cylinders) colored according to *A*. (*C*) Ribbon diagram of the (crystallographic) BDV-M tetramer, highlighting the tesselation of the L-shaped monomers.

The 2 open sides of the β-sandwich are closed by helix α3, 2 loops, and the N-terminal part of the polypeptide chain on one side, and by helix α4 on the other. A search for structurally homologous proteins using the DALI server (22) yielded only 1 match of statistical significance, the N-terminal domain of the full length M-protein VP40 (17) (Fig. S1), despite a sequence identity of only 10%. Monomeric VP40 is composed of 2 structurally related domains of 200 (N-terminal) and 125 (C-terminal) residues (17), to which BDV-M exhibits rmsds of 1.8 Å (61 matched residues) and 2.1 Å (48 matched residues), respectively; the latter value is comparable with superposition of the VP40 N- and C- terminal domains themselves (1.8 Å for 56 matched residues). BDV-M and the VP40 N-terminal domain differ mainly in the lengths and orientation of loops and helices; interestingly, octameric structures of the VP40 N-terminal domain, found to bind RNA oligonucleotides (18), diverge from that of monomeric VP40 in the same regions (Fig. S1).

Oligomeric Architecture of BDV-M. BDV-M crystallizes in space group I432 with 1 monomer in the asymmetric unit (23); a tightly-assembled, noncovalently-linked tetramer is formed by crystallographic 4-fold symmetry (Fig. 1*C*). The BDV-M tetramer forms a square planar arrangement of dimensions 84 × 84 × 42 Å. Square planar tetramers are comparably rare for biological macromolecules; interestingly, the nucleoprotein of BDV also forms square planar tetramers with dimensions 59 × 59 × 87 Å (24). The L-shaped BDV-M monomer tessellates to form the compact tetramer; every long arm of the L interacts with the short arm of the next monomer. Analysis of the solvent-accessible areas shows that ≈26% (2,315 Å^2) of the surface area (8,869 Å^2) of each monomer is buried in the tetramer by the 2 neighboring monomers.

The C-terminal portion of one monomer interacts with the N termini and the external surface of β-sheet II of the next monomer. Helix α4, located at the center of the tetramer, interacts with the external surface of β-sheet I, helix α4, and the surrounding loop of the second monomer (Fig. 1*C*). Near the 4-fold axis, residues Glu-108 and Lys-111 at the beginning of helix α4 appear to play a special role in stabilization of the tetramer. Although residue Glu-108 exhibits multiple conformations, pointing in one case toward the surface of the tetramer, its side chain is in the other case buried and forms salt bridges to Lys-111 of a neighboring monomer. The BDV-M tetramer is held together by further hydrophobic and polar interactions, with a total of 50 hydrogen bonds and 150 van der Waals contacts formed by each monomer.

The dominant form of BDV-M isolated from infected horses is tetrameric (15), suggesting that it is the tetramer that binds to the viral membrane, and flotation experiments have shown that BDV-M binds to membranes of BDV-infected cells (14). The interaction of the purified BDVM tetramer with brain polar lipid extract was studied by using the monolayer technique (25). Injection of the protein results in a clear decrease in lipid monolayer surface pressure (Fig. S2), suggesting a condensation of the lipid phase akin to that of the binding of polybasic and polyaliphatic peptides to negatively-charged lipids such as phosphatidylserine (25, 26). To delineate the putative membrane binding surface, the electrostatic potential distribution was calculated (Fig. 2*A*). One face of the BDV-M tetramer displays a highly positively-charged surface, with small negatively-charged patches corresponding to isolated amino acids from the C termini. This face is also rich in solvent-exposed hydrophobic and aromatic side chains. The combination of these characteristics suggests that this face is responsible for membrane interactions (27) (Fig. 2*B*). The opposite face of the BDV-M tetramer reveals 2 positively-charged S-shaped patches that cross each other at the tetramer center, separated by negatively-charged areas (see Fig. 4*B*), whereas the tetramer edges exhibit alternating patches of acidic/basic nature (Fig. 2*B*) that could mediate lateral association to form the planar arrays observed previously (16).

In the crystal lattice, each tetramer is positioned face-to-face with a second tetramer via the putative membrane binding surface to form a weakly-associated crystallographic octamer. A positively-charged patch around Arg-98 of 1 tetramer juxtaposes the negatively-charged patch near the C terminus of the opposing tetramer. Because of the disk-like shape of the BDV-M tetramer, distances between the tetramers range from 3.95 Å (Pro 142 O–Arg 98 NE), through 6–8 Å at the edges, up to 20–25 Å between their centers, resulting in large solvent channels with dimensions 35 × 35 × 35 Å. Interactions between the 2 tetramers are mediated by solvent molecules, including SO_4^{2-} ions. This finding is consistent with experimental results showing that higher oligomeric states of the M-protein appear after long incubation at high salt concentration and ultracentrifugation studies confirming that an equilibrium exists between tetramers and octamers of BDV-M (16). Because the membrane binding face is not accessible within the crystallographic octamer, it is unlikely that it is able to bind to lipid bilayers.

Electron Density Reveals Nucleotide Binding to BDV-M. During the structure determination, additional electron density was found near to the C terminus of helix α4, close to the 4-fold axis of the BDV-M tetramer. The density could be interpreted as a pyrimidine mononucleotide, which we have assigned as cytidine-5′-monophosphate (Fig. 3). The base is sandwiched in a pocket between the side chains of Phe-37 (from loop β1–β2) and His-112 (of helix α4) at a distance of 3.4 Å to each (Fig. 3*A*); such

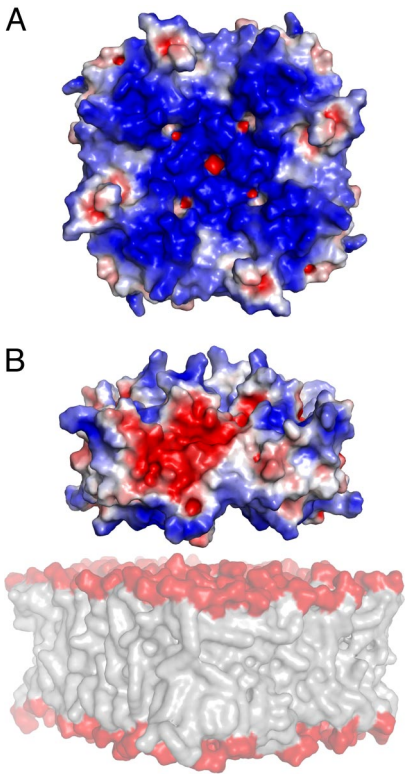

Fig. 2. Surface properties of the putative membrane-binding face of the BDV-M tetramer. (*A*) The electrostatic surface potential reveals this face to be highly basic (areas colored in white, red, and blue denote neutral, negative, and positive potential contoured at 0, − 3, and +3 kT/e, respectively). View is rotated 180° around the horizontal axis relative to Fig. 1*C*. (*B*) Side view of the tetramer, obtained by rotating (*A*) by 90° about a horizontal axis, depicting BDV-M approaching a phospholipid membrane (*Lower*). The alternating surface charges (acidic/basic) of the tetramer edges would facilitate lateral assembly to form planar arrays.

a parallel ring stacking between bases and aromatic residues is typical for protein–nucleic acid interactions (28). A series of hydrogen bonds to the base are observed: between the main-chain atoms of Phe-37 and the base ring of the nucleotide, from the side chain of Gln-36, from the side chain of Asn-115$^{\#}$ of a symmetry-related molecule and a water-mediated hydrogen bond to Asn-39 N, and the side chain of Asn 115$^{\#}$ (Fig. 3*A*). In addition, the O2′ atom of a riboxynucleotide sugar moiety would hydrogen-bond to the side chain of Gln-36. The network of interactions observed for the cytosine base would be similar for uracil, with an extra hydrogen bond for the uracil N3 hydrogen. Binding of thymine is also conceivable, although the methyl group would make close contacts to the side chain of Asn-115$^{\#}$. In contrast to these pyrimidine bases, neither the size of the pocket nor the hydrogen-bonding pattern is suited to the binding of the bulky purine bases adenine and guanine. Surprisingly, RNA binding occurs on a face of the monomer opposite to that corresponding to the trinucleotide binding site in VP40 octamers (18) (Fig. S1 and Fig. S3).

Binding of Oligonucleotides to BDV-M. In previous work, UV spectra of BDV-M oligomeric fractions showed 2 maxima with a ratio OD_{280} to OD_{260} of ≈1.1 (16), suggesting the presence of nucleic acid. Although the density described above is clear, showing that a pyrimidine base is bound to the heterologously produced BDV-M near the tetramer axis, the limited resolution and high overall *B* value of the data does not allow differentiation between RNA and DNA. Furthermore, the 4-fold averaging imposed by the crystallographic symmetry precludes identification of longer oligonucleotides that do not follow this symmetry. The electrostatic distribution at the protein surface suggests, however, that BDV-M could also bind larger nucleic acid fragments (Fig. 4).

Freshly-prepared BDV-M was analyzed to investigate both the type and length of oligonucleotides bound to the protein. Nucleic acids isolated from BDV-M were alternatively radioactively-labeled at the 5′ and 3′ ends and analyzed by using urea-PAGE (Fig. 4*A*). 5′ Labeling using T4 polynucleotide kinase (PNK), which can label both DNA and RNA nucleotides, shows a strong band corresponding to a 16-nt fragment. Digestion with RNase T_1 followed by urea-PAGE separation reveals degradation of the nucleic acid fragments, providing evidence that the nucleic acid in question is indeed RNA. 3′ Labeling using polyadenylate polymerase (PAP), specific for ssRNA nucleotides, reveals 13- and 16-nt fragments. RNase treatment of the sample also results in degradation of the nucleic acid fraction, although the ensuing fragments are larger than for the digested 5′-labeled PNK

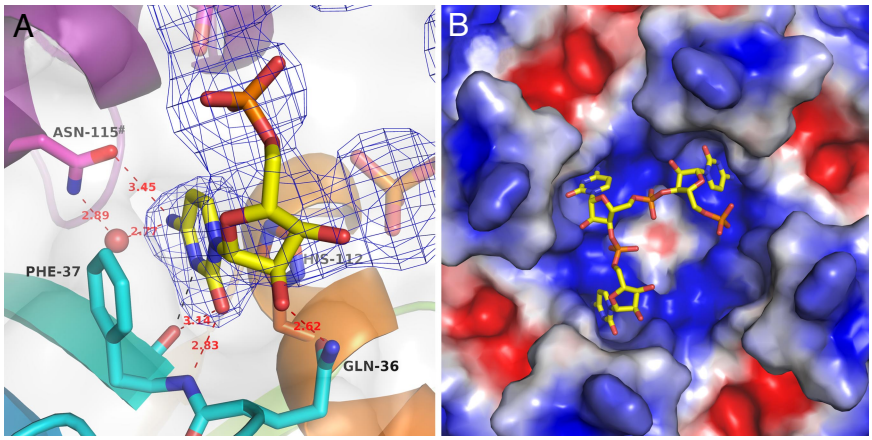

Fig. 3. The nucleotide binding site in BDV-M. (*A*) Experimental electron density (omit map contoured at 3 σ) with refined monoribonucleotide cytidine-5′-monophosphate at the interface between 2 monomers (view and colors as in Fig. 1*C*). The pyrimidine ring is sandwiched between the side chains of Phe 37-and His-112 and is held in position through hydrogen bonds to the main chain of Phe-37 and the carboxamide group of the neighboring Asn-115 (distances in Å). In addition, the O2′ atom of a riboxynucleotide sugar moiety would hydrogen-bond to the side chain of Gln 36. (*B*) Electrostatic potential surface of BDV-M (contour levels as in Fig. 2) with refined RNA trinucleotide (CCC). Note the alternative positions of the phosphate groups in the crystallographically 4-fold averaged structure.

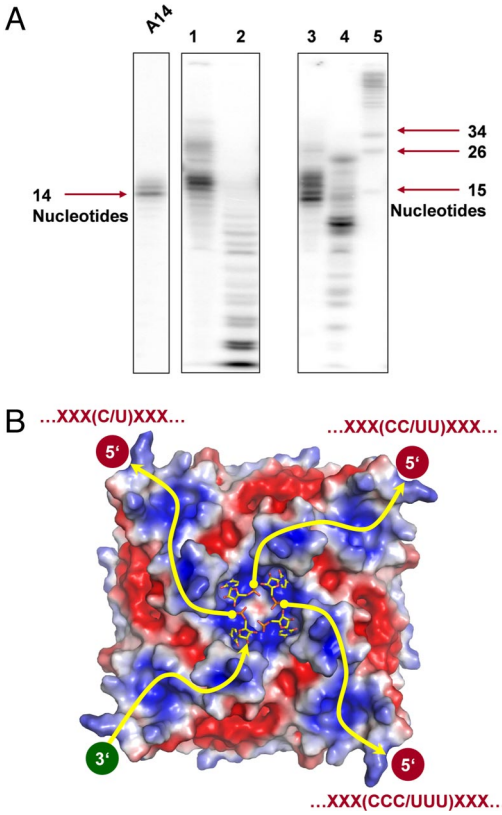

Fig. 4. Heterologously-expressed BDV-M binds ssRNA oligonucleotides. (*A*) Urea-PAGE of isolated nucleic acid from purified BDV-M tetramer. Left lane, defined 14-nt polyadenine marker; lane 1, isolated RNA labeled at the 5′ terminus using PNK; lane 2, as lane 1 after RNase T_1 digestion; lane 3, isolated RNA labeled at the 3′-terminus using PAP; lane 4, as lane 3 after RNase T_1 digestion; lane 5, polyadenine marker. These results prove the copurification of heterologously expressed BDV-M tetramer with RNA oligonucleotides of ≈16 nt. (*B*) Schematic depiction of possible binding mode of ssRNA. A distinctive basic patch along the tetramer diagonals could accommodate the polyphosphate backbone (yellow arrows), such that an incoming chain (3′-end bottom left) ends with the observed bound nucleotide (center). Assuming a specificity for cytidine/uridine, there are 3 possible exit routes for the 5′-end: (*i*) at the top left, with 1 pyrimidine base bound near the tetramer axis; (*ii*) at the top right, with 2 nt; and (*iii*) at the bottom right, with 3 central bases contributing to specificity. It is not possible to distinguish between them because of the 4-fold crystallographic symmetry.

sample. Pretreatment of the BDV-M protein fraction with either RNase A or the dual specific endonuclease Benzonase before nucleic acid isolation gave equivalent results, showing that the RNA oligonucleotide is protected by the M-protein. Conversely, attempts to remove the nucleic acid via denaturation of BDV-M and subsequent in vitro folding were unsuccessful until now, raising the possibility that RNA binding plays a structural role in the integrity of the tetramer. Treatment of both the 3′- and 5′-labeled isolated nucleic acid samples with RNase A yielded almost complete digestion to mononucleotides. Thus, both labeling strategies provide evidence that BDV-M expressed heterologously in *Escherichia coli* binds and protects ssRNA oligonucleotides with a length of ≈16 bases or more.

Combining the crystallographic and in vitro data, it is likely that the BDV-M tetramer binds RNA oligonucleotides containing 1, 2, or 3 consecutive pyrimidine bases; 4 bases cannot be bound simultaneously because of steric restraints (Fig. 4*B*). For a better understanding and more realistic view of RNA bound to the BDV-M tetramer, we modeled and refined a cytidine trinucleotide by linking 3 symmetry-related CMP molecules (Fig. 3*B*) in 2 possible orientations: 3′–5′ and 5′–3′. Only 1 orientation of the trinucleotide could be refined to fit the electron density map with reasonable geometry and protein contacts without increasing the crystallographic *R* factors. Conformational parameters for the refined mononucleotide and trinucleotide are presented in Table S1. Refinement as a trinucleotide alters the nucleotide conformation compared with the mononucleotide model slightly: although the pyrimidine bases barely change their positions, locations of the phosphate groups and sugar moieties change as a consequence of the covalent linkage of the mononucleotides. The largest shifts are observed for the 5′ nucleotide, whose pyrimidine ring is shifted ≈0.5 Å and free phosphate group moved 2.2 Å compared with the mononucleotide refinement. Similar results are obtained upon refinement of a dinucleotide.

The refined triribonucleotide model fits well to the (4-fold crystallographically averaged) electron density and allows tentative interpretation of weak residual electron density close to each terminal phosphate group as belonging to preceding and following nucleotides. Inspection of the BDV-M electrostatic potential indicates a possible course for longer polynucleotide chains along the surface of the tetramer (Fig. 4*B*), corroborated by the locations of bound sulfate ions in the crystal. For minimal strain in the ssRNA near the tetramer axis, a single BDV-M tetramer should bind an oligoribonucleotide segment containing 2 consecutive pyrimidine bases, although other binding modes (1 nucleotide or 3 consecutive bases) are also feasible (Fig. 4*B*). It is possible that further RNA specificity pockets are present on the surface, but are undetectable at the present stage of our investigations.

The exposed nature of ssRNA binding suggested by the present structure is quite different to that observed in octamers of the VP40 N-terminal domain (18), where the oligonucleotides are threaded through the axial octameric pore between adjacent dimeric molecules (Fig. S3). Electrostatic potential distributions of the VP40 octamers are also compatible with the nucleotide binding mode described here, however. Conversely, superposition of the VP40 trinucleotide on the BDV-M tetramer suggests that the Ebola RNA binding mode (on the BDV-M membrane binding surface) is also feasible, such that the crystallographic BDV-M octamer could encapsulate RNA oligonucleotides.

Discussion

The data presented here reveal the structure of a full-length NSV M-protein. Despite a lack of any significant sequence homology among NSV M-proteins, BDV-M exhibits a striking resemblance to the 2 domains of VP40 (17). This conservation of 3D structure in the absence of any recognizable evolutionary relationship is reminiscent of the situation for retroviral M-proteins (29). However, the structures of BDV-M and VP40 are clearly different to those of other NSVs. Although VSV-M also consists largely of β-sheet (19), its topology is unrelated, whereas influenza-M1 is entirely α-helical (20). Despite functional and structural homology with VP40, membrane binding modes appear to differ significantly between the 2 viruses. VP40 has been observed in multiple oligomeric forms; oligomerization occurs via the N-terminal domain to form monomeric, dimeric, hexameric, and octameric species (10, 17, 18, 30–32). In contrast, BDV-M has been observed in only 2 oligomeric states (15, 16), namely tetramers and octamers.

The primary role assigned to M-proteins is the attachment of nucleocapsids to cellular membranes, essential for viral assembly and budding. As postulated for other M-proteins (20, 29), the basic face of the BDV-M tetramer, interspersed with surface exposed aliphatic and aromatic residues, could facilitate membrane targeting and/or binding, consistent with membrane binding capabilities of the BDV-M tetramer (16). VP40 membrane

binding is affected by the C-terminal domains in the hexameric state (9, 33) in an as-yet-unknown manner.

M-proteins have also been shown to play a role in the replication of a number of NSVs: M-proteins inhibit viral transcription in rabies (34), VSV (35), influenza (36), respiratory syncytial virus (37), and other viruses (38–40). In persistently BDV-infected cells, BDV-M can be found both in the cytoplasm and the nuclei of infected cells (41), where it colocalizes with viral proteins N (nucleocapsid protein), P (phosphoprotein), and X, suggesting that the M-protein is an integral component of the viral RNP (41). Although BDV-M copurifies with affinity-purified N (42), binding studies indicate that M interacts not with N but with the viral P protein, so that M-RNP association is thought to be mediated by the P protein (41). Our data suggest that M–RNP complex formation driven via the RNA-binding properties of the BDV-M tetramer could reconcile this apparent contradiction.

Direct binding of RNA has also been reported for other NSV M-proteins, including influenza A (43, 44), Ebola (10, 18, 31), and respiratory syncytial viruses (45). Crystal structures of nucleoprotein–RNA complexes from rabies (46) and VSV (47) reveal ring-like oligomers with the RNA almost completely protected. Recombinantly-expressed rabies oligomers contain 9–13 protomers (48); within the virus, however, the nucleocapsid forms a coil containing ≈53 protomers per helical turn (49). It has been demonstrated for VSV that condensation of the nucleocapsid is mediated by VSV-M (50, 51). Should RNA binding be a universal feature of NSV M-proteins, it is conceivable that nucleocapsid condensation is facilitated by M binding to viral RNA segments between adjacent nucleoprotein–RNA rings.

As a result of their compact genome, it is essential for viruses to maximize the functionality of individual gene products. BDV possesses the smallest and most compact genome of all viruses in the *Mononegavirales* order, and monomeric BDV-M is the smallest among all NSV M-proteins. In contrast to the 2-domain VP40 (17), in which the N-terminal domain governs oligomerization and the C-terminal domain directs membrane binding (10), all M-protein functions must be performed by using the single domain BDV-M. We show here that, in addition to interacting with lipid membranes, the BDV-M tetramer is able to bind RNA concomitantly, with implications for RNP formation, nucleocapsid targeting, and viral maturation. Although VP40 N-terminal domain octamers have also been shown to bind ssRNA (18), the interaction with oligonucleotides is fundamentally different to that observed for BDV-M. It is conceivable that other VP40 states (homooligomeric and/or heterooligomeric) could result in M–RNA complexes topologically similar to that described here. Octameric VP40 forms only in the presence of ssRNA (31) and may be involved in viral replication. Similarly, in associating with RNA without membrane-binding capacity, the BDV-M octamer could participate in RNP formation and function. Further structural studies will help elucidate the multiple roles of M-proteins during the viral life cycle, including processes of viral entry, replication, localization, assembly, maturation, and budding from the host cell.

Methods

X-Ray Crystal Structure Solution. Selenomethionine-labeled BDV-M was prepared and crystallized as described (23). The asymmetric unit with 1 BDV-M monomer contains 3 selenomethionines. The structure was solved by using 3-wavelength multiple wavelength anomalous dispersion (*SI Text* and Table S2) with data collected at the BW6 beamline at the Deutsches Elektronen Synchrotron (Hamburg, Germany). The final model consists of residues 3–142, 1 RNA nucleotide (interpreted as cytidine-5′-monophosphate), 3 sulfate ions, and 30 water molecules, with values of R_{work} and R_{free} of 21.72% and 26.64%, respectively (Table 1). No interpretable electron density could be found for the remaining N-terminal residues, which are most likely disordered.

Table 1. Refinement statistics

Refinement	$\lambda_1 = 0.9792$
Resolution range, Å	20–2.65 (2.77–2.65)
Completeness (working + test), %	98.2 (95.4)
No. of reflections, $F > 0$	7491 (897)
Wilson B, Å^2	75.3
R_{cryst}, %*	21.72 (27.50)
R_{free}, %†	26.64 (27.80)
No. of nonhydrogen atoms	
Protein	1,182
Water	39
Sulphate	15
Cytidine-5′-monophosphate	26
rmsd from ideality	
Bond lengths, Å	0.007
Bond angles, °	1.40
Dihedral angles, °	23.3
Improper angles, °	0.88
Average B factor, Å^2	
Protein atoms	61.59
Main chain	60.55
Water	59.85
Cytidine-5′-monophosphate	83.78
SO_4	54.4

Values in parentheses correspond to the highest resolution shell.
*$R_{cryst} = \Sigma||F_{obs}| - |F_{calc}|| / \Sigma |F_{obs}|$.
†R_{free} is calculated as R_{cryst} for a test set comprising 7.5% reflections not used in the refinement.

Expression and Purification of BDV-M. Expression of the full-length BDV-M gene and purification of the BDV-M-maltose binding protein fusion protein was performed as described (16). Maltose binding protein affinity chromatography was carried out by using an ÄKTA FPLC System (Amersham Biosciences). Further purification and separation of the fusion tag after factor Xa cleavage was carried out by using size exclusion chromatography via a HiLoad 26/60 Superdex 75 column (Amersham Biosciences). Amicon Ultra Centrifugal Filter Units (Millipore) were used for final concentration of the purified BDV-M.

Monolayer Experiments. Brain polar lipid extract (porcine) was purchased from Avanti Polar Lipids and used without further purification. Surface pressure measurements were performed by using a homebuilt film balance with a circular Teflon trough (surface area of 7 cm^2 and subphase volume of 11 mL). The surface pressure was measured with the Wilhelmy plate method (Riegler & Kirstein). The subphase was an ultrapure aqueous buffer solution (50 mM Hepes, 25 mM NaCl, pH 7.6). The lipid mixture was dissolved in chloroform and spread at the air/water interace with a microsyringe to give initial surface pressures between 12 and 32 mN/m. Surface films were equilibrated for at least 30 min, after which the protein was injected into the subphase and the surface pressure change was recorded. The final trough concentration of the BDV-M tetramers in each experiment was 100 nM. Experiments were performed at 20 ± 0.5 °C in a closed container to keep the air humidity constant, with continuous stirring of the subphase with a magnetic stirring bar.

Isolation of Nucleic Acid. The copurified nucleic acids were separated from protein as follows: 100 μL of protein solution were diluted with 100 μL of proteinase K buffer (Merck) and digested by 20 μL of proteinase K (Merck) at 50 °C for 30–45 min. Phenol/chloroform (220 μL; 1:1) were added to 220 μL of the proteinase K reaction mixture to dissociate nucleic acids and protein fragments. After vortexing and centrifugation for 30 min at 19,000 × g, the upper aqueous phase was extracted a second time with 1 vol chloroform. The nucleic acid isolate was then purified by ethanol precipitation. One microliter of glycogen (20 mg/mL; Roche), one-third 10 M ammonium acetate, and 10 vol absolute ethanol were added and centrifuged for 20 min at 19,000 × g. The pellet was washed with 50 μL of 70% ethanol by centrifugation at 19,000 × g. The precipitate was dissolved in 20 μL of diethylpyrocarbonate (DEPC) in H_2O and stored at −20°C.

Radioactive Labeling and RNase Digestion. The enzyme PAP was used to radiolabel the 3′ end of ssRNA fragments. A 50-μL reaction contained 25 μL of

2× PAP buffer (New England Biolabs), 0.5 μL of RNasin (Promega), 1 μL of 25 mM DTT (Roth), 1 μL of 50 mM $MnCl_2$ (Merck), 1 μL of DEPC H_2O, 20 μL of nucleic acid isolate, 1 μL of α^{32}P-cordecypin triphosphate (Amersham Bioscience), and 0.5 μL of PAP (New England Biolabs). PNK was used for the 5′ labeling. Five microliters of 10× PNK buffer (New England Biolabs), 0.5 μL of RNasin (Promega), 0.5 μL of 100 mM CDP (Sigma), 5 μL of 500 nM ATP (Sigma), 17.5 μL of DEPC H_2O, 20 μL of nucleic acid isolate, 1 μL of $\gamma[^{32}]$ATP (Amersham Bioscience), and 0.5 μL of PNK (New England Biolabs) were added. Both reactions were incubated for 1 h at 37 °C.

An RNase digestion was also carried out to differentiate between RNA and DNA. Sixteen microliters of RNase buffer (20 mM Tris, 100 mM NaCl, pH 8.0), 3 μL of radiolabeled nucleic acid, and 1 μL of RNase T_1 (25 units/μL; Roth) were incubated for 30 min at 30 °C.

Urea-PAGE of Nucleic Acids. The RNase digestion reaction was stopped by adding 30 μL of 5× formamide buffer (10 mL of formamide, 10 mg of xylencyanol, 10 mg of bromophenol blue, 200 μL of 0.5 M EDTA). 0.5 μL of samples of PAP- and PNK-labeling reaction were mixed with 9.5 μL of 5× formamide buffer. All samples were boiled for 5 min at 95 °C. Separation of 10-μL prepared samples was carried out in a 20% acrylamide/50% urea gel at 40-W power with an electrophoresis buffer containing 90 mM Tris, 90 mM boric acid, and 1 mM EDTA.

ACKNOWLEDGMENTS. We thank Galina Kachalova and Hans Bartunik of the Max-Planck-Gesellschaft for providing beam-time and valuable experimental assistance at beamline BW 6 of Deutsches Elektronen Synchrotron Hamburg, Elmar Wahle (Institut für Biochemie, Martin-Luther-Universität Halle-Wittenberg) for useful advice concerning the nucleotide labeling assays, Alfred Blume (Institut für Chemie, Martin-Luther-Universität Halle-Wittenberg) for discussions concerning the monolayer experiments, and Christiane Herden (Institut für Veterinär-Pathologie, Justus-Liebig-Universität Gießen) for helpful discussions on the manuscript. This work was supported by the Deutsche Forschungsgemeinschaft Graduiertenkollegs 541 ''Proteinfunktion auf atomarer Ebene'' (W.G. and M.T.S.) and 1026 ''Conformational transitions in macromolecular interactions'' (M.T.S.).

1. de la Torre JC (2006) Reverse-genetic approaches to the study of Borna disease virus. *Nat Rev Microbiol* 4:777–783.
2. Richt JA, Rott R (2001) Borna disease virus: A mystery as an emerging zoonotic pathogen. *Vet J* 161:24–40.
3. Staeheli P, Sauder C, Hausmann J, Ehrensperger F, Schwemmle M (2000) Epidemiology of Borna disease virus. *J Gen Virol* 81:2123–2135.
4. Hilbe M, et al. (2006) Shrews as reservoir hosts of Borna disease virus. *Emerg Infect Dis* 12:675–677.
5. Dürrwald R, Kolodziejek J, Herzog S, Nowotny N (2007) Meta-analysis of putative human bornavirus sequences fails to provide evidence implicating Borna disease virus in mental illness. *Rev Med Virol* 17:181–203.
6. Hornig M, Solbrig M, Horscroft N, Weissenbock H, Lipkin WI (2001) Borna disease virus infection of adult and neonatal rats: Models for neuropsychiatric disease. *Curr Top Microbiol Immunol* 253:157–177.
7. Schwemmle M, Carbone KM, Tomonaga K, Garten W, Nowotny N (2005) in *Virus Taxonomy, Classification, and Nomenclature of Viruses: 8th Report of the International Committee on Taxonomy of Viruses*, eds Fauquet CM, et al. (Academic, San Diego), pp 615–622.
8. Garoff H, Hewson R, Opstelten DJE (1998). Virus maturation by budding. *Microbiol Mol Biol Rev* 62:1171–1190.
9. Scianimanico S, et al. (2000) Membrane association induces a conformational change in the Ebola virus matrix protein. *EMBO J* 19:6732–6741.
10. Timmins J, Ruigrok RW, Weissenhorn W (2004) Structural studies on the Ebola virus matrix protein VP40 indicate that matrix proteins of enveloped RNA viruses are analogues but not homologues. *FEMS Microbiol Lett* 233:179–186.
11. Gaudin Y, et al. (1997) Conformational flexibility and polymerization of vesicular stomatitis virus matrix protein. *J Mol Biol* 274:816–825.
12. Chong LD, Rose JK (1994) Interactions of normal and mutant vesicular stomatitis virus matrix proteins with the plasma membrane and nucleocapsids. *J Virol* 68:441–447.
13. Baudin F, Petit I, Weissenhorn W, Ruigrok RW (2001) In vitro dissection of the membrane and RNP binding activities of influenza virus M1 protein. *Virology* 281:102–108.
14. Kraus I, et al. (2001) Open reading frame III of Borna disease virus encodes a nonglycosylated matrix protein. *J Virol* 75:12098–12104.
15. Stoyloff R, et al. (1997) The glycosylated matrix protein of Borna disease virus is a tetrameric membrane-bound viral component essential for infection. *Eur J Biochem* 246:252–257.
16. Kraus I, Bogner E, Lilie H, Eickmann M, Garten W (2005) Oligomerization and assembly of the matrix protein of Borna disease virus. *FEBS Lett* 579:2686–2692.
17. Dessen A, Volchkov V, Dolnik O, Klenk HD, Weissenhorn W (2000) Crystal structure of the matrix protein VP40 from Ebola virus. *EMBO J* 19:4228–4236.
18. Gomis-Ruth FX, et al. (2003) The matrix protein VP40 from Ebola virus octamerizes into pore-like structures with specific RNA binding properties. *Structure (London)* 11:423–433.
19. Gaudier M, Gaudin Y, Knossow M (2002) Crystal structure of vesicular stomatitis virus matrix protein. *EMBO J* 21:2886–2892.
20. Sha B, Luo M (1997) Structure of a bifunctional membrane-RNA binding protein, influenza virus matrix protein M1. *Nat Struct Biol* 4:239–244.
21. Harris A, Forouhar F, Qiu S, Sha B, Luo M (2001) The crystal structure of the influenza matrix protein M1 at neutral pH: M1–M1 protein interfaces can rotate in the oligomeric structures of M1. *Virology* 289:34–44.
22. Holm L, Sander C (1997) Dali/FSSP classification of three-dimensional protein folds. *Nucleic Acids Res* 25:231–234.
23. Kraus I, et al. (2002) Crystallization and preliminary X-ray analysis of the matrix protein of Borna disease virus. *Acta Crystallogr D* 58:1371–1373.
24. Rudolph MG, et al. (2003) Crystal structure of the Borna disease virus nucleoprotein. *Structure (London)* 11:1219–1226.
25. Maget-Dana R (1999) The monolayer technique: A potent tool for studying the interfacial properties of antimicrobial and membrane-lytic peptides and their interactions with lipid membranes. *Biochim Biophys Acta* 1462:109–140.
26. Shafer PT (1974) The interaction of polyamino acids with lipid monolayers. *Biochim Biophys Acta* 373:425–435.
27. Mulgrew-Nesbitt A, et al. (2006) The role of electrostatics in protein-membrane interactions. *Biochim Biophys Acta* 1761:812–826.
28. Allers J, Shamoo Y (2001) Structure-based analysis of protein–RNA interactions using the program ENTANGLE. *J Mol Biol* 311:75–86.
29. Christensen AM, Massiah MA, Turner BG, Sundquist WI, Summers MF (1996) Three-dimensional structure of the HTLV-II matrix protein and comparative analysis of matrix proteins from the different classes of pathogenic human retroviruses. *J Mol Biol* 264:1117–1131.
30. Hartlieb B, Weissenhorn W (2006) Filovirus assembly and budding. *Virology* 344:64–70.
31. Hoenen T, et al. (2005) VP40 octamers are essential for Ebola virus replication. *J Virol* 79:1898–1905.
32. Nguyen TL, et al. (2005) An all-atom model of the pore-like structure of hexameric VP40 from Ebola: Structural insights into the monomer-hexamer transition. *J Struct Biol* 151:30–40.
33. Ruigrok RWH, et al. (2000) Structural characterization and membrane binding properties of the matrix protein VP40 of Ebola virus. *J Mol Biol* 300:103–112.
34. Finke S, Mueller-Waldeck R, Conzelmann KK (2003) Rabies virus matrix protein regulates the balance of virus transcription and replication. *J Gen Virol* 84:1613–1621.
35. Clinton GM, Little SP, Hagen FS, Huang AS (1978) The matrix (M) protein of vesicular stomatitis virus regulates transcription. *Cell* 15:1455–1462.
36. Watanabe K, Handa H, Mizumoto K, Nagata K (1996) Mechanism for inhibition of influenza virus RNA polymerase activity by matrix protein. *J Virol* 70:241–247.
37. Ghildyal R, Baulch-Brown C, Mills J, Meanger J (2003) The matrix protein of human respiratory syncytial virus localizes to the nucleus of infected cells and inhibits transcription. *Arch Virol* 148:1419–1429.
38. Cornu TI, de la Torre JC (2001) RING finger Z protein of lymphocytic choriomeningitis virus (LCMV) inhibits transcription and RNA replication of an LCMV S-segment minigenome. *J Virol* 75:9415–9426.
39. Reuter T, Weissbrich B, Schneider-Schaulies S, Schneider-Schaulies J (2006) RNA interference with measles virus N, P, and L mRNAs efficiently prevents and with matrix protein mRNA enhances viral transcription. *J Virol* 80:5951–5957.
40. Ogino T, Iwama M, Ohsawa Y, Mizumoto K (2003) Interaction of cellular tubulin with Sendai virus M protein regulates transcription of viral genome. *Biochem Biophys Res Commun* 311:283–293.
41. Chase G, et al. (2007) Borna disease virus matrix protein is an integral component of the viral ribonucleoprotein complex that does not interfere with polymerase activity. *J Virol* 81:743–749.
42. Mayer D, Baginsky S, Schwemmle M (2005) Isolation of viral ribonucleoprotein complexes from infected cells by tandem affinity purification. *Proteomics* 5:4483–4487.
43. Wakefield L, Brownlee GG (1989) RNA-binding properties of influenza A virus matrix protein M1. *Nucleic Acids Res* 17:8569–8580.
44. Ye Z, Liu T, Offringa DP, McInnis J, Levandowski RA (1999) Association of influenza virus matrix protein with ribonucleoproteins. *J Virol* 73:7467–7473.
45. Rodriguez L, Cuesta I, Asenjo A, Villanueva N (2004) Human respiratory syncytial virus matrix protein is an RNA-binding protein: Binding properties, location, and identity of the RNA contact residues. *J Gen Virol* 85:709–719.
46. Albertini AAV, et al. (2006) Crystal structure of the rabies virus nucleoprotein-RNA complex. *Science* 313:360–363.
47. Green TJ, Zhang X, Wertz GW, Luo M (2006) Structure of the vesicular stomatitis virus nucleoprotein–RNA complex. *Science* 313:357–360.
48. Schoehn G, Iseni F, Mavrakis M, Blondel D, Ruigrok RW (2001) Structure of recombinant rabies virus nucleoprotein–RNA complex and identification of the phosphoprotein binding site. *J Virol* 75:490–498.
49. Albertini AAV, Schoehn G, Weissenhorn W, Ruigrok RWH (2008) Structural aspects of rabies virus replication. *Cell Mol Life Sci* 65:282–294.
50. Newcomb WW, Brown JC (1981) Role of the vesicular stomatitis virus matrix protein in maintaining the viral nucleocapsid in the condensed form found in native virions. *J Virol* 39:295–299.
51. Newcomb WW, Tobin GJ, Mcgowan JJ, Brown JC (1982) In vitro reassembly of vesicular stomatitis virus skeletons. *J Virol* 41:1055–1062.